

**Classification:** Engineering in Physical Sciences

***Directional Pumping of Water and Oil Microdroplets on Slippery Surface***

Jieke Jiang<sup>a, 1</sup>, Jun Gao<sup>b, 1</sup>, Hengdi Zhang<sup>a</sup>, Wenqing He<sup>a</sup>, Jiangqiang Zhang<sup>a</sup>, Dan Daniel<sup>c</sup>,  
and Xi Yao<sup>a, 2</sup>

<sup>a</sup> Department of Biomedical Sciences, City University of Hong Kong, 83 Tat Chee Avenue, Kowloon, Hong Kong SAR, P. R. China; <sup>b</sup> Physics of Complex Fluids, University of Twente, Enschede 7500, The Netherlands; and <sup>c</sup> Institute of Materials Research and Engineering, 2 Fusionopolis Way, Singapore 138634

<sup>1</sup> J.J. and J.G. contributed equally to this work.

<sup>2</sup> To whom correspondence should be addressed. E-mail: xi.yao@cityu.edu.hk

**Keywords:** droplet-transport, microdroplet, capillary force, slippery surface, anti-fouling

**Author contributions:** X.Y. conceived the concept and supervised the research. X.Y. and J.J. designed the experiments. J.J., H.Z. and W.H. performed the research. J.G. and D.D. set up models and carried out the calculation. J.J., J.G., H.Z., W.H., J.Z., D.D. and X.Y. wrote the manuscript.

The authors declare no conflict of interest.

## **Abstract**

Transporting water and oil microdroplets is important for applications ranging from water harvesting to biomedical analysis, but remains a great challenge. This is due to the amplified contact angle hysteresis and insufficient driving force in the micrometer scale, especially for low surface energy oil droplets. Coalescence of neighboring droplets which releases vast additional surface energy was often required, but its relatively uncontrollable nature brings uncertainties to the droplet motion and the methodology is not applicable to single droplet. Here we introduce a new strategy based on slippery surface with immobilized lubricant menisci to directionally transport microdroplets. By simply mounting hydrogel dots on slippery surface, the raised menisci remotely pump microdroplets via capillary force with high efficiency, regardless of droplet size or surface energy. By proof-of-concept experiments, we demonstrate that our method allows for highly efficient water droplet collection and highly sensitive biomedical analyte detection.

## **Significance Statement**

This work designed a strategy to directionally transport water and oil microdroplets. By simply mounting hydrogel dots on a slippery surface to arrest lubricant menisci, spontaneously formed capillary force pumps liquid microdroplets continuously at high efficiency. Enabled by the nature of capillary force, such strategy is universally applicable to water and oil droplets of different surface tensions, and to droplets with different sizes, yet with little substrate preparation effort. We expect this to be useful in many applications including heat exchangers, water harvesters, biomedical devices, and more.

Directional transport of water and oil droplets without external energy input is crucial in a variety of applications (1), such as microfluidics (2, 3), heat exchangers (4), biomedical analysis (5, 6), and water harvesting (7). The most successful strategies to transport droplets are often inspired by the remarkable liquid-collection capabilities of insects and plants, which exploit either a surface energy gradient or an asymmetric geometry to generate a driving force (8-13). However, these strategies generally fail in transporting droplets with diameters of several hundred micrometers or less. This is because at such a small scale, contact angle hysteresis becomes increasingly important, while the external driving forces become negligible (14). This challenge is particularly difficult to address for oil droplets transport, because most solid surfaces are oleophilic, which dramatically increases the hysteresis.

To address this challenge, there are two optional approaches: either to enhance the driving force or to reduce the contact angle hysteresis. Coalescence of neighboring droplets can be used to generate this enhanced driving force, since the reduction in surface area releases additional energy for work, but its wide adoption is precluded by its largely uncontrollable nature, and its inapplicability for single droplets (7, 15-18). Alternatively, employing surfaces with low contact angle hysteresis is a promising approach. Recently, directional driving of oil droplets was demonstrated on a textured oleophobic surface (12), but this strategy requires complicated substrate design and fabrication. A simpler approach is to introduce a liquid layer on a solid material which results in a defect-free fluid interface with extreme slipperiness to both water and oil, the so-called slippery liquid-infused surface (19). For example, a recent study successfully demonstrated the directional transport of small water droplets on slippery surface with asymmetric bumps (20). However, continuous growth of droplets via condensation or coalescence was still needed to derive sufficient driving force and driving oil droplets remains challenging.

Nature has a smart way to transport small objects on liquid surface. For example, seeds of aquatic plants can be collected by surface-piercing vegetation via capillary force (21, 22), a

crucial process in seed dispersal (Fig. 1a). Some water-walking insects, particularly the larva of waterlily leaf beetle, proves an excellent example of using directional capillary force to transport itself on the curved menisci from water to dry land (23). The capillary driving strategy is effective for objects with sizes ranging from nanometer to millimeter (24). Herein, inspired by nature, we demonstrate the directional capillary pumping of microdroplets on slippery surfaces, without the need of coalescence or continuous growth (Fig. 1b). The maximum pumping distance is determined by capillary length, which is independent to the size and surface tension of droplet, and feature size of mounted hydrogel dots. This enables an unprecedentedly easy and robust strategy to transport different-sized water and oil droplets with minimum substrate preparation.

## **Results**

The slippery surface was made of polydimethylsiloxane (PDMS) infused with silicone oil. Surface-piercing hydrogel dots were inkjet-printed onto the PDMS using a liquid patterning method (25) before infusing with oil (Fig. 1c). After oil infusion (oil thickness is typically 20  $\mu\text{m}$ ), the hydrogel dots were surrounded by oil menisci, which served as immobilized spots to capture microdroplets (Fig. 1d, see details in the Supplementary Fig. S1). After fabrication, the substrate was tilted, and Fig. 1e and f show that water droplets within  $\sim 1$  mm distance are driven toward the hydrogel dots against gravity, confirming the effectiveness of our droplet transport strategy. It is noteworthy that the hydrogel dots can be replaced by a glass slide, a glass bead or any other surface-piercing structures that raise the lubricant meniscus with similar results (Fig. S2 in the supporting information). To verify that the driving force is capillarity, we removed the oil meniscus by wiping the lubricant off the surface. Since the capillary force is bridged by the meniscus, this should suppress the capillary force and indeed, the droplets can no longer be pumped upwards (compare Fig. 1e and 1g, 1f and 1h).

A simplified model can help to rationalize the driving force and the resultant motion, as sketched in Fig. 1i (extract from Supplementary Movie S1) and j. We define  $\alpha$  and  $\beta$  as the slope angles of the oil menisci to the left and right side of the droplet, respectively. Due to the overlapping and thus elevated oil menisci between the droplet and the hydrogel dot, there is a difference between  $\alpha$  and  $\beta$  ( $\alpha > \beta$ ), generating an attractive capillary force  $F_c > 0$  which drive the microdroplet to the hydrogel dot:  $F_c = \gamma R(\cos\beta - \cos\alpha) > 0$ , where  $\gamma$  is the oil/air interfacial tension and  $R$  is the droplet size (26-28). At the initial stage when the moving velocity  $U$  is low,  $F_c$  is balanced by the viscous drag force  $F_d \sim \eta RU$ , where  $\eta = 10$  mPa·s is the oil viscosity. Therefore,  $U \sim \gamma / \eta (\cos \beta - \cos \alpha)$ , where  $\gamma/\eta \approx 2$  m/s is the characteristic visco-capillary velocity. This model is in agreement with our measured values of  $(\cos \beta - \cos \alpha)$  and  $U$  of a 0.3 mm diameter droplet during the driving process (Fig. 1k). The slope (dashed line in Fig. 1k) is 0.05 m/s, which suggests a prefactor of about 0.03 in our model, whereas the classical Stokes flow predicts a prefactor of  $1/4\pi \approx 0.08$  (29). This slight disagreement is expected since classical Stokes flow does not account for the wall-effect due to the PDMS substrate and the finite gap between the droplet and the hydrogen dot. We also note that in our system the size of the menisci is comparable to that of the droplet, which was not the case in previous analyses on the viscous dissipation of droplets on slippery surfaces (30, 31).

The maximum droplet driving distance  $D_{max}$  is determined by the meniscus length, which we found experimentally to be given by its capillary length  $\lambda = (\gamma/\rho g)^{1/2} = 1.5$  mm (Fig. 2a), where  $\rho$  is the oil density and  $g$  is the acceleration due to gravity (32).  $F_c$  (and hence also  $\cos \beta - \cos \alpha$ ) is a function of the distance between hydrogel and droplet  $L$ . Previous work establishes that  $F_c$  decays exponentially for large  $L \gg \lambda$  and increases dramatically with decreasing  $L$  when  $L \sim \lambda$  (27, 28), consistent with our experimental observations (Fig. S3 in the supporting information).

It is important to note that  $\lambda$  is only dependent on the properties of the infused oil ( $\rho, \gamma$ ). This suggests a unique advantage of capillary pumping strategy: it is highly robust and is

insensitive to the structure of substrate material and the geometrical, physical or chemical properties of droplets.

To test this, we first observed the driving process of 100 droplets with diameters ranging from 0.2 to 1.2 mm deposited with syringe. Regardless of the diameter, those droplets deposited beyond  $D_{max} \approx 1.5$  mm mostly failed to be driven while those deposited closer than  $D_{max}$  were successfully driven (Fig. 2b). Large droplets with a size of 5 mm was also observed to be successfully driven (Fig. S4). To test the driving of extremely small droplets, we sprayed aerosolized water droplet with a diameter of  $\sim 0.1$  mm on the surface and visualized the successful driving (Fig. S5). Our capillary pumping strategy should be applicable to all droplet sizes, but smaller droplets are difficult to generate reliably and thereby not tested. Furthermore, we also investigated the driving capability on hydrogel dots with different sizes and droplets of different surface tensions. Results show that  $D_{max}$  stays at around 1.5 mm, and is relatively insensitive to the diameter of hydrogel dots (Fig. 2c). The surface tension of water can be tuned from 72 mN/m to 47 mN/m by adding different concentrations of ethylene glycol (EG). Within this range, the maximum driving distance  $D_{max}$  was kept at  $\sim 1.5$  mm (Fig. 2d). This result remains true even for micro oil droplets despite their low surface tensions. Fig 2e-g show that pure EG (47 mN/m), olive oil (32 mN/m), and 3M Fluorinert FC-70 (18 mN/m) droplets at  $\sim 1.5$  mm away were driven towards the hydrogel dots within a few seconds, even though they have low contact angles. Our capillary pumping strategy is therefore universally applicable to all liquid droplets immiscible with the infused oil. Replacing silicone oil infused PDMS with fluorinated oil infused slippery surface (19), which is immiscible with most common liquids, will make this strategy applicable to an even wider range of liquids. Compared to previously reported self-propelled droplet transporting strategies (Fig. S6 and Table S1 in the supporting information), only our strategy allows the driving of both water and oil droplets with sub-millimeter sizes without the need of coalescence. The minimum size of the droplet that can be driven successfully is also among the smallest. Thanks to the low

hysteresis nature of our slippery surface, our strategy also resulted in the highest reported driving speed ( $\sim 10$  mm/s) when compared to previous strategies (Fig. S6).

Another remarkable feature of our method is its continuous driving capability. For traditional methods that rely on geometric asymmetry or surface tension gradient, the driving capability is disabled once the asymmetric or gradient region is covered by collected droplets (7). However, for our method, the fluidic oil meniscus is regenerated after each droplet collection, exerting continuous capillary forces to surrounding droplets. Fig. 3a shows three water droplets that were driven to the hydrogel dot in sequence. The continuous driving capability of microdroplets due to the hydrogel dots is highly beneficial to water collection. As a proof-of-concept, aerosol water droplets were sprayed onto the surface (Supplementary Movie S2) and the droplet collection efficiency was characterized. For comparison, the same amount of water was sprayed onto another lubricated PDMS surface without the hydrogel dots. With the presence of the hydrogel dots, aerosol droplets were rapidly and continuously driven toward the hydrogel dots (Fig. 3b, and schematic illustration in the inset of Fig. 3c). Due to the rapid driving, the fraction of droplet covered area reached less than 10% immediately after spraying, and then quickly decreased to  $\sim 2\%$  (Fig. 3c). In contrast, the fraction of area covered by droplets PDMS surface without the dots reached 20% immediately after spraying (left image in Fig. 3d, and Fig. 3e) and decreased gradually to about 15% after a few seconds due to random coalescence of neighboring droplets (middle and right images of Fig. 3d, and schematic illustration in the inset of Fig. 3e). The highly efficient droplet collection should be highly beneficial for droplet condensation and fog harvesting. Importantly, the hydrogel dots can also be patterned in large area for larger scale collection of microdroplets (Fig. 3f and Supplementary Movie S3).

Furthermore, we demonstrate that the high efficiency aerosol droplets collection can be used in highly sensitive biomedical analysis. Detecting aerosol analytes, such as pathogen-containing respiratory aerosolized droplets (33-35), remains a great challenge due to the small

droplet size and low concentration. Our capillary pumping method can significantly enrich analytes onto the hydrogel dots, which substantially increases the detection sensitivity (Fig. 4a). As a demonstration, we sprayed aerosol green fluorescent protein (GFP)-tagged *Escherichia coli* (*E. coli*, a bacteria) on our substrate. Fluorescence images show that 4 s after spraying, *E. coli* can be hardly detected (Fig. 4b). The fluorescent signal (averaged over the vertical positions) is low and widely distributed (Fig. 4d). However, after 50 s, microdroplets containing *E. coli* aggregated by the hydrogel dot at the center, show strong and centered fluorescent signal (Fig. 4c and d). Notably, the fluorescent intensity was increased by nearly an order of magnitude. For practical applications, it could be helpful to use patterned arrays of hydrogel dots to realize multi-site enrichment and analysis (Supporting Information Fig. S7). Bacterial killing can also be realized by pre-immobilizing biocides on the hydrogel dots (Supporting Information Fig. S8). Highly sensitive label-free detection could also be realized if combined with other analytical method such as Raman spectroscopy or mass spectrometry.

In summary, we developed a new strategy for directional transport of microdroplets on slippery liquid-infused surfaces. Single microdroplets could be transported and collected by capillary pumping. Such strategy is unprecedentedly easy and highly robust. To our best knowledge, this is the first strategy that can drive both oil and water microdroplet with sub-millimetric sizes. This strategy could be used in applications including fog harvesting, droplet condensation, and highly sensitive biomedical analysis. We envision that, by adopting active surface (36), for example, by incorporating patterned smart hydrogel dots whose shape responses to external stimuli, or even by creating complex surface-piercing structures with ferrofluids in magnetic field, it is possible to fabricate smart droplet fluidic devices.

## Methods

**Material Fabrication.** 4wt% sodium alginate (Sigma-Aldrich) solution was printed onto thermally curable PDMS precursor (Dow Corning Sylgard 184, 10: 1 base and curing agent). PDMS precursor was spin-coated on a clean glass slide at a rotating speed of 3000 rpm. A dispensing system (Biodot, AD1520) was applied to print alginate sodium solution on liquid PDMS precursor film. The resulted sample was annealed at 80 °C for 5 h before immersed into a 500 mM CaCl<sub>2</sub> solution for 0.5 h for the gelation of hydrogel dots. Then the PDMS film was immersed into silicone oil (10cSt, Sigma-Aldrich) for 5 hours to swell the PDMS and form an immobilized lubricant meniscus. To control the thickness of the over-coated layer, the oil on the surface was gently wiped by filter papers and the same oil with controlled volume was added to a known surface area of the sample. GFP-expressing *E. coli* was used in the test of bacterial collection and detection.

**Characterization.** Microdroplets were generated by two methods: the spraying method and the single droplet method. For the spraying method, a thin film chromatography sprayer (Sigma Aldrich, 250 mL) was used to generate the microdroplets. The sprayer was placed at about 15 cm distance to the surface and sprayed for one time in a single experiment. Alternatively, microdroplets with controlled diameter were generated individually by a homemade superhydrophobic needle. The microdroplet movements were recorded by a horizontally placed microscope equipped with a high-speed CCD (Olympus, i-speed 3). The fluorescent images in the collection and detection of bacteria were acquired by fluorescent microscope (Leica MZ10F Fluorescent Stereomicroscope and Nikon Eclipse Ni-E Fluorescent Microscope).

Further details on the methods are available in the Supplementary Information.

## **Acknowledgements**

The authors thank the financial support by the National Natural Science Foundation of China (Grant No. 21501145), the General Research Fund (GRF) Hong Kong (Grant No. 21214215) and financial support from City University of Hong Kong.

## References

1. Liu M, Wang S, & Jiang L (2017) Nature-inspired superwettability systems. *Nature Reviews Materials* 2(7):17036-17052.
2. Lv JA, *et al.* (2016) Photocontrol of fluid slugs in liquid crystal polymer microactuators. *Nature* 537(7619):179-184.
3. Cira NJ, Benusiglio A, & Prakash M (2015) Vapour-mediated sensing and motility in two-component droplets. *Nature* 519(7544):446-450.
4. Daniel S, Chaudhury MK, & Chen JC (2001) Fast drop movements resulting from the phase change on a gradient surface. *Science* 291(5504):633-636.
5. Jokinen V, Leinikka M, & Franssila S (2009) Microstructured Surfaces for Directional Wetting. *Adv Mater* 21(47):4835-4838.
6. Chu KH, Xiao R, & Wang EN (2010) Uni-directional liquid spreading on asymmetric nanostructured surfaces. *Nat Mater* 9(5):413-417.
7. Ju J, *et al.* (2012) A multi-structural and multi-functional integrated fog collection system in cactus. *Nature Communications* 3:1247-1252.
8. Ichimura K, Oh SK, & Nakagawa M (2000) Light-driven motion of liquids on a photoresponsive surface. *Science* 288(5471):1624-1626.
9. Chaudhury MK & Whitesides GM (1992) How to Make Water Run Uphill. *Science* 256(5063):1539-1541.
10. Chen HW, *et al.* (2016) Continuous directional water transport on the peristome surface of *Nepenthes alata*. *Nature* 532(7597):85-89.
11. Malvadkar NA, Hancock MJ, Sekeroglu K, Dressick WJ, & Demirel MC (2010) An engineered anisotropic nanofilm with unidirectional wetting properties. *Nat Mater* 9(12):1023-1028.
12. Li J, *et al.* (2016) Oil droplet self-transportation on oleophobic surfaces. *Science Advances* 2(6):e1600148-e1600153.
13. Prakash M, Quere D, & Bush JWM (2008) Surface tension transport of prey by feeding shorebirds: The capillary ratchet. *Science* 320(5878):931-934.
14. Wang QB, Yao X, Liu H, Quere D, & Jiang L (2015) Self-removal of condensed water on the legs of water striders. *Proceedings of the National Academy of Sciences of the United States of America* 112(30):9247-9252.
15. Cho HJ, Preston DJ, Zhu YY, & Wang EN (2017) Nanoengineered materials for liquid-vapour phase-change heat transfer. *Nature Reviews Materials* 2(2):16092-16108.
16. Zheng Y, *et al.* (2010) Directional water collection on wetted spider silk. *Nature* 463(7281):640-643.
17. Liu J, *et al.* (2016) Guided Self-Propelled Leaping of Droplets on a Micro-Anisotropic Superhydrophobic Surface. *Angewandte Chemie* 55(13):4265-4269.
18. Boreyko JB & Chen CH (2009) Self-Propelled Dropwise Condensate on Superhydrophobic Surfaces. *Physical Review Letters* 103(18):1845011-1845014.
19. Wong TS, *et al.* (2011) Bioinspired self-repairing slippery surfaces with pressure-stable omniphobicity. *Nature* 477(7365):443-447.
20. Park KC, *et al.* (2016) Condensation on slippery asymmetric bumps. *Nature* 531(7592):78-82.
21. Peruzzo P, Defina A, Nepf HM, & Stocker R (2013) Capillary Interception of Floating Particles by Surface-Piercing Vegetation. *Physical Review Letters* 111(16):164501.

22. Peruzzo P, Defina A, & Nepf H (2012) Capillary trapping of buoyant particles within regions of emergent vegetation. *Water Resources Research* 48(7):W07512.
23. Hu DL & Bush JWM (2005) Meniscus-climbing insects. *Nature* 437(7059):733-736.
24. Pokroy B, Kang SH, Mahadevan L, & Aizenberg J (2009) Self-Organization of a Mesoscale Bristle into Ordered, Hierarchical Helical Assemblies. *Science* 323(5911):237-240.
25. Jiang JK, *et al.* (2016) Fabrication of Transparent Multilayer Circuits by Inkjet Printing. *Adv Mater* 28(7):1420-1426.
26. Cavallaro M, Botto L, Lewandowski EP, Wang M, & Stebe KJ (2011) Curvature-driven capillary migration and assembly of rod-like particles. *Proceedings of the National Academy of Sciences of the United States of America* 108(52):20923-20928.
27. Paunov VN, Kralchevsky PA, Denkov ND, & Nagayama K (1993) Lateral capillary forces between floating submillimeter particles. *Journal of Colloid and Interface Science* 157(1):100-112.
28. Danov KD, Pouligny B, & Kralchevsky PA (2001) Capillary forces between colloidal particles confined in a liquid film: The finite-meniscus problem. *Langmuir* 17(21):6599-6609.
29. Batchelor GK (2000) *An introduction to fluid dynamics* (Cambridge university press).
30. Daniel D, Timonen JVI, Li RP, Velling SJ, & Aizenberg J (2017) Oleoplaning droplets on lubricated surfaces. *Nature Physics* 13(10):1020-1025.
31. Keiser A, Keiser L, Clanet C, & Quere D (2017) Drop friction on liquid-infused materials. *Soft Matter* 13(39):6981-6987.
32. Schellenberger F, *et al.* (2015) Direct observation of drops on slippery lubricant-infused surfaces. *Soft Matter* 11(38):7617-7626.
33. Sorrell EM, Wan HQ, Araya Y, Song HC, & Perez DR (2009) Minimal molecular constraints for respiratory droplet transmission of an avian-human H9N2 influenza A virus. *Proceedings of the National Academy of Sciences of the United States of America* 106(18):7565-7570.
34. Zhang QY, *et al.* (2013) H7N9 Influenza Viruses Are Transmissible in Ferrets by Respiratory Droplet. *Science* 341(6144):410-414.
35. Imai M, *et al.* (2012) Experimental adaptation of an influenza H5 HA confers respiratory droplet transmission to a reassortant H5 HA/H1N1 virus in ferrets. *Nature* 486(7403):420-428.
36. Wang W, *et al.* (2018) Multifunctional ferrofluid-infused surfaces with reconfigurable multiscale topography. *Nature* 559(7712):77-82.
37. Bai H, *et al.* (2010) Direction Controlled Driving of Tiny Water Drops on Bioinspired Artificial Spider Silks. *Adv Mater* 22(48):5521-5525.
38. Ju J, Xiao K, Yao X, Bai H, & Jiang L (2013) Bioinspired Conical Copper Wire with Gradient Wettability for Continuous and Efficient Fog Collection. *Adv Mater* 25(41):5937-5942.
39. Kajiya T, *et al.* (2016) Cylindrical chains of water drops condensing on microstructured lubricant-infused surfaces. *Soft Matter* 12(46):9377-9382.
40. Bai H, *et al.* (2011) Large-Scale Fabrication of Bioinspired Fibers for Directional Water Collection. *Small* 7(24):3429-3433.
41. Li K, *et al.* (2013) Structured cone arrays for continuous and effective collection of micron-sized oil droplets from water. *Nature Communications* 4:2276-2282.
42. Deng S, *et al.* (2017) Controlled droplet transport to target on a high adhesion surface with multi-gradients. *Scientific reports* 7:45687.
43. Wang T, *et al.* (2018) Controlling Directional Liquid Motion on Micro-and Nanocrystalline Diamond/ $\beta$ -SiC Composite Gradient Films. *Langmuir* 34(4):1419-1428.

44. Hernandez SC, *et al.* (2013) Chemical gradients on graphene to drive droplet motion. *Acs Nano* 7(6):4746-4755.
45. Ito Y, *et al.* (2007) The movement of a water droplet on a gradient surface prepared by photodegradation. *Langmuir* 23(4):1845-1850.
46. Banuprasad TN, *et al.* (2017) Fast transport of water droplets over a thermo-switchable surface using rewritable wettability gradient. *ACS applied materials & interfaces* 9(33):28046-28054.
47. Wu H, *et al.* (2017) Smart design of wettability-patterned gradients on substrate-independent coated surfaces to control unidirectional spreading of droplets. *Soft matter* 13(16):2995-3002.
48. Bliznyuk O, Jansen HP, Kooij ES, Zandvliet HJ, & Poelsema B (2011) Smart design of stripe-patterned gradient surfaces to control droplet motion. *Langmuir* 27(17):11238-11245.

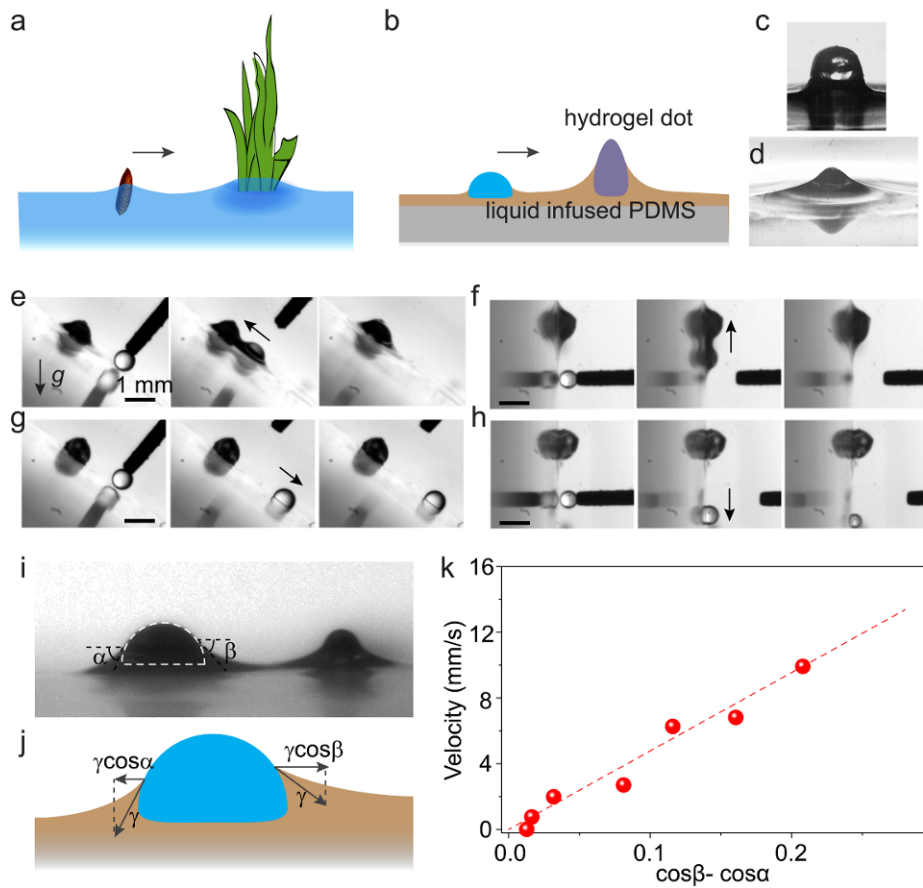


**Fig. 1 Directionally pumping droplets by capillary force on slippery surface with immobilized meniscus.** (a) Schematic shows surface-piercing vegetation capturing floating seeds by capillary force. (b) Inspired by this, capillary pumping of microdroplets on slippery surface with immobilized meniscus is developed, whereby meniscus-immobilizing hydrogel dot capture nearby droplets by capillary force. (c) Hydrogel dot was printed on PDMS surface. (d) After infusing the surface with silicone oil, the hydrogel dot raises and immobilizes oil meniscus. (e-f) Mediated by the meniscus, water microdroplet can be pumped to the hydrogel dot against gravity, whether the slippery surface is tilted by 45 degree (e) or 90 degree (f). (g-h) In contrast, microdroplets cannot be driven without the oil meniscus. (i) Optical images showing a microdroplet (left) being driven toward the hydrogel dot (right), bridged by the oil meniscus. (j) The driving force is due to the net surface tension force projected on the horizontal direction ( $\gamma \cos \beta - \gamma \cos \alpha$ ) exerted on the opposite sides of the droplet. (k)  $\cos \beta - \cos \alpha$  and the velocity of the droplet follow a nearly linear relationship.

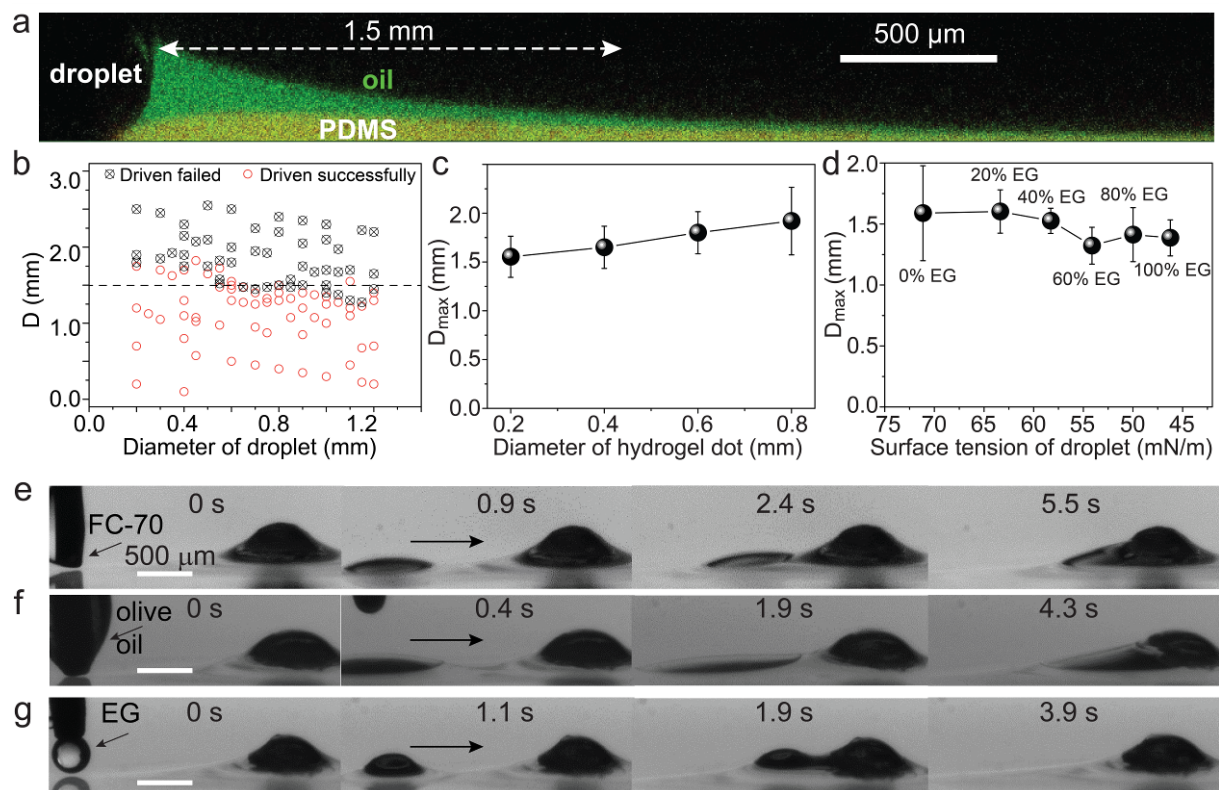


**Fig. 2 Water and oil microdroplets can be robustly driven.** The driving capability is dependent on the oil meniscus, with the maximum driving distance approximately equal to the meniscus length, i.e. the capillary length ( $\lambda$ ). (a) Confocal fluorescence image showing the green-dyed oil meniscus, with a length approximately equal to  $\lambda=1.5$  mm. (b) Results for 100 microdroplets with different diameters and different distance ( $D$ ) to the hydrogel dot, showing that the maximum driving distance ( $D_{max}$ ) is around 1.5 mm (dashed line). (c)  $D_{max}$  stays at around 1.5-2.0 mm for various hydrogel dot diameters. (d)  $D_{max}$  is around 1.5 mm for droplets of different surface tensions from 72 to 47 mN/m, which is obtained by adding different ratio of ethylene glycol (EG) to water. (e-g) Low surface tension oil droplets, including Fluorinert FC-70, olive oil, and EG, with a distance of  $\sim 1.5$  mm can also be driven to the hydrogel dot in a few seconds.

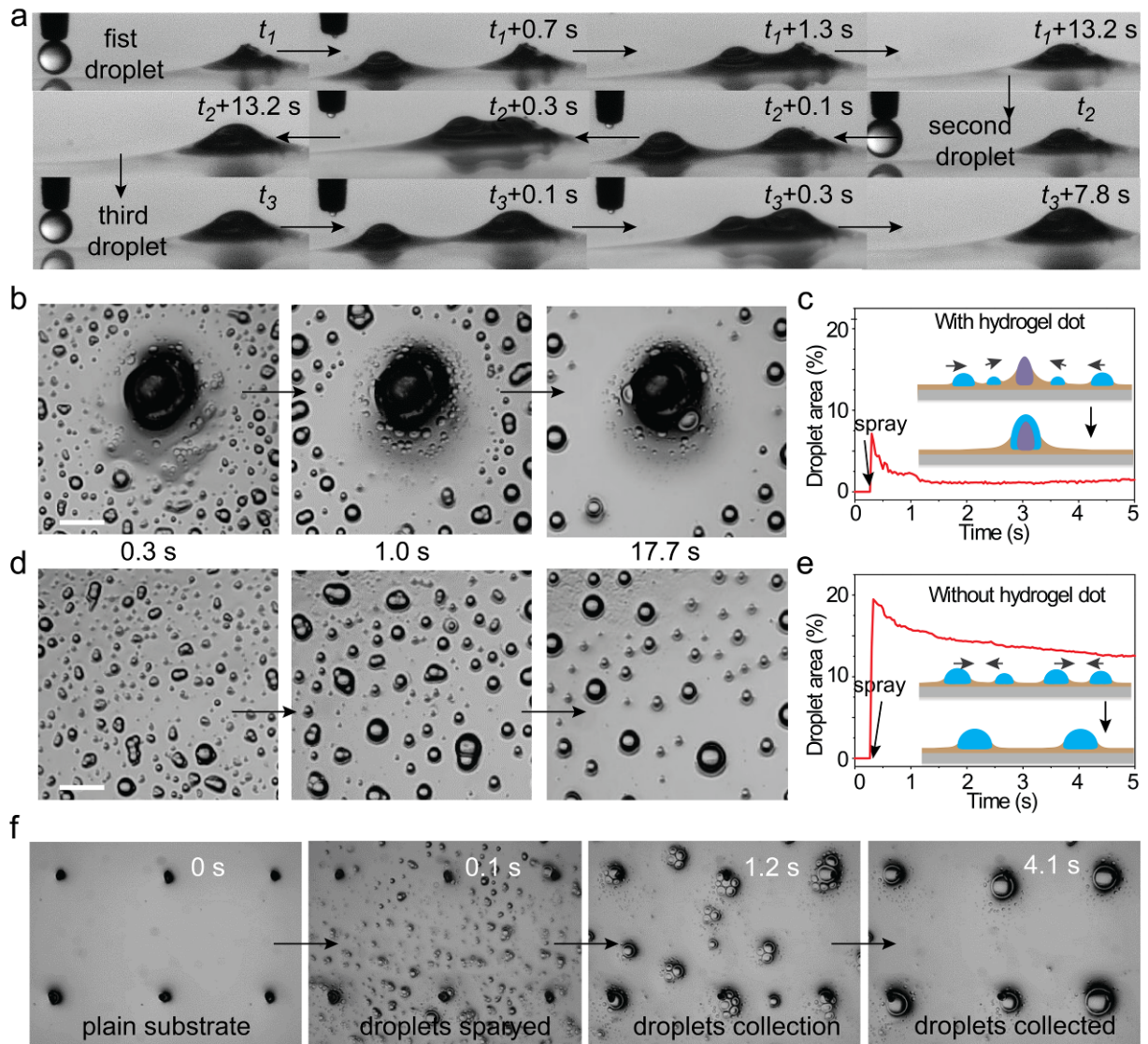


**Fig. 3 Continuous capillary pumping for high efficiency droplet collection.** (a) Thanks to the self-regeneration of oil meniscus after each droplet collection, microdroplets can be continuously pumped to the hydrogel dot. The optical images show three water droplets driven to the hydrogel dot in sequence. (b) The continuous microdroplet pumping enables high efficiency water droplet collection. Optical images show that almost all sprayed aerosol microdroplets near the hydrogel dot were rapidly and sequentially pumped to hydrogel dot. (c) As a result, the area fraction covered by droplet kept low, and gradually decreased to  $\sim 2\%$  after spraying. (d) On the contrary, without hydrogel dot, the sprayed aerosol microdroplets randomly coalesced. (e) The resultant area fraction covered by droplet is much higher. (f) Hydrogel dots can be patterned into arrays for larger scale droplet collection.

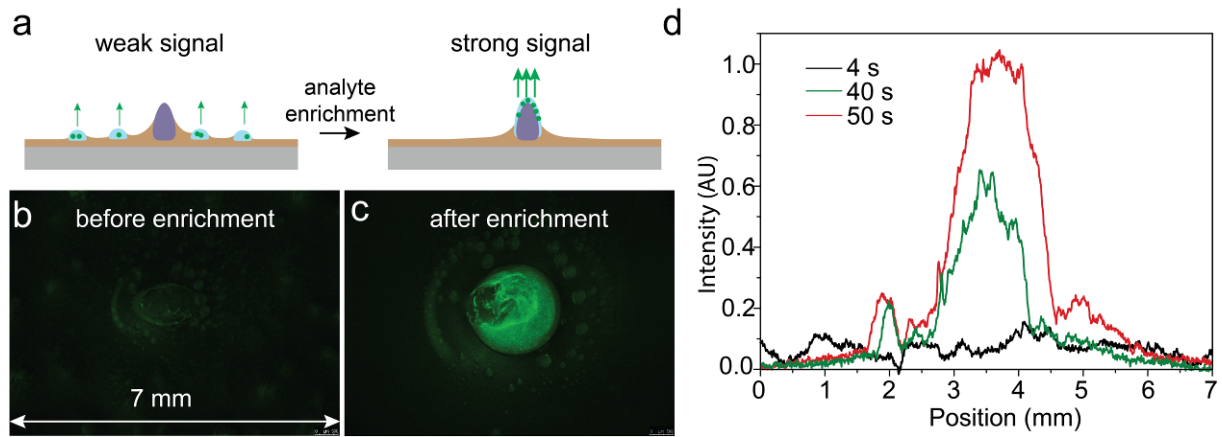


**Fig. 4 Highly sensitive detection of aerosol biomedical analyte enabled by the high efficiency droplet collection.** (a) Schematic illustration showing the detection method. Aerosol droplets containing biomedical analytes are collected by the hydrogel dots, which substantially enriches the analytes, thereby greatly increasing the sensitivity. (b) Sprayed aerosol GFP-expressing *E. coli* (green) showed weak fluorescence intensity. (c) After the aerosol droplets were collected by the hydrogel dots (center), *E. coli* was enriched at the center and showed strong fluorescence intensity. (d) Average intensity vs position at different time after spraying.

Supporting Information

***Directional Pumping of Water and Oil Microdroplets on Slippery Surface***

Jieke Jiang<sup>a, 1</sup>, Jun Gao<sup>b, 1</sup>, Hengdi Zhang<sup>a</sup>, Wenqing He<sup>a</sup>, Jiangqiang Zhang<sup>a</sup>, Dan Daniel<sup>c</sup> and Xi Yao<sup>a, 2</sup>

<sup>a</sup> Department of Biomedical Sciences, City University of Hong Kong, 83 Tat Chee Avenue, Kowloon, Hong Kong SAR, P. R. China; <sup>b</sup> Physics of Complex Fluids, University of Twente, Enschede 7500, The Netherlands; and <sup>c</sup> Institute of Materials Research and Engineering, 2 Fusionopolis Way, Singapore 138634

<sup>1</sup> J.J. and J.G. contributed equally to this work.

<sup>2</sup> To whom correspondence should be addressed. E-mail: xi.yao@cityu.edu.hk

## 1. Experimental Details

*Spraying microdroplets.* A thin film chromatography sprayer (250 mL, Sigma Aldrich) was used to generate the microdroplets. The gas flow of compressed air was generated by squeezing the rubber pump of the sprayer with a customized actuator. The distance between the sprayer and the sample was set at 15 cm.

*Generation of single microdroplets.* A steel needle with flat top and inner diameter of 60  $\mu\text{m}$  was used to fabricate a superhydrophobic needle. The needle was immersed into a solution formulated by dissolving 1 g fumed silica (22 nm, Sigma-Aldrich) and 1 g PDMS precursor (10: 1 base and curing agent) in 15 ml n-hexane for several times to overcoat a superhydrophobic layer on the needle. By using the superhydrophobic needle, the squeezed microdroplets will not adhere on the tip of the needle, which can facilitate the control of the droplet diameter. The superhydrophobic needle was mounted on a three-dimensional mobile platform with a universal joint. A microliter syringe (500  $\mu\text{L}$ , Hamilton) filled with deionized water was connect with the needle by a plastic tubing. The volume of the droplet generated by the needle was controlled by a syringe pump (KDS 100, KDS Scientific). For the generation of tiny oil droplet, the FC-70 and olive oil will adhere on the needle due to their low surface tension. However, those oil droplets were still able to detach from the needle when contact with the slippery surface because of the low surface tension of the superhydrophobic needle.

*Confocal microscope imaging of the oil meniscus.* The cross section of the oil meniscus was imaged using Zeiss LSM 880 laser confocal microscope. The solid PDMS was stained with Nile red (J & K Scientific) by a swelling method. Nile red was dissolved in ethanol to form a 200 mM solution. 100  $\mu\text{L}$  of this solution was dispensed into 20 mL silicone oil. The as-prepared silicone oil was used to swell a solid PDMS for 5 hours. Then, the lubricant layer on the surface was thoroughly washed by pure silicone oil without dye. Then the surface was carefully wiped by a filter paper. Silicone oil stained with coumarin-6 (J & K Scientific)

prepared by the same procedure was used to form the lubricant layer. Certain volume of silicone oil stained with coumarin-6 was over-coated on the wiped surface with known area. The as prepared substrate was used for confocal characterization. After each capturing, a confocal Z-stacking mode was applied to visualize the cross section of the oil meniscus.

*Preparation of bacterial medium.* GFP-tagged *E. coli* was used in the bacterial collection test and bactericidal test. A single colony of *E. coli* on a solid Luria-Bertani (LB) agar plate was transferred to 30 mL of liquid LB culture medium and was grown at 37°C for 12 hours. Bacteria were harvested by centrifugation (7100 rpm for 2 min), and then washed twice with sterilized phosphate-buffered saline (PBS) solution. The supernatant was discarded and the pellet was re-suspended in 30 ml sterilized PBS solution. This suspension of *E. coli* was used as the medium for generating bacteria-containing microdroplets. These microdroplets were sprayed on the testing surfaces and characterized with fluorescent microscope (Leica MZ10F Fluorescent Stereomicroscope). For the capturing of fluorescent images, the microscope was focused to the slippery surface at the bottom of the hydrogel dot under visible light. Then the microscope was switched to GFP channel to capture the driven process of bacteria. To measure the fluorescent signal of the collected bacteria, a rectangle covers the collected bacterial media on the hydrogel dot was chosen as the measuring area. The width of the rectangle equals to the diameter of the collected droplet while its length equals to 7 mm. The fluorescent intensity at different position of  $x$ -axis is obtained by calculating the average signal on  $y$ -axis.

*Loading of biocide onto the Hydrogel Dots.* A slippery surface with hydrogel dot array were immersed into 5 mM solution of thyme essential oil for seconds and was took out slowly. The biocide solution adhered on the hydrogel dots forming droplet array. Before testing, the substrate was allowed to dry at room temperature for 0.5 hour. The bacteria medium stained

with bacterial viability kit was sprayed to the surface and the substrate was subsequently sent for fluorescence microscope observation (Nikon Eclipse Ni-E Fluorescent Microscope).

*LIVE/DEAD BacLight bacterial viability assay.* For the bactericidal test, a LIVE/DEAD BacLight bacterial viability kit (L7007, Thermo Fisher Scientific) was used to assess the bacterial cell viability of the collected *E. coli* on the hydrogel dot. In this assay, the red-fluorescent nucleic acid staining agent propidium iodide, which only penetrates damaged cell membrane, was used to label dead bacterial cells. 3  $\mu$ L of propidium iodide was added to 10 mL of above obtained *E. coli* medium at room temperature and was kept in the dark for 15 min before used as the spraying solution.

*Measurement of driving velocity in references.* The driving velocity of this bio-inspired capillary pumping system is compared with that of other bio-inspired droplet driven systems. The first driven system is the cone-shaped structure (including spider-silk-inspired fiber and cactus-spine-inspired needle) followed by two driven systems mainly inspired from pitch plant including nanostructured slippery surface and slippery asymmetric bump. The highest velocity stated in references (37-39) are used for comparison. For references (7, 16, 20, 40, 41) that no velocity is provide, the average velocity is calculated and used for the comparison.

Choosing of the highest velocity and data processing of the average velocity are described as following. The driving velocity of reference (7) is the average velocity calculated based on its Figure 2e. The driving velocity of reference (16) is the average velocity calculated based on its Figure 2g. The driving velocity of reference (20) is the average velocity calculated based on its Figure 3d and Figure 4b. The driving velocity of reference (37) is the highest velocity stated in the paper (please see its Figure 3a). The driving velocity of reference (38) is the highest velocity stated in the paper (please see its Figure 3d). The driving velocity of reference (39) is the highest velocity stated in the paper (please see its Figure 4b). The driving velocity of reference (40) is the average velocity calculated based on its Figure 5. The driving velocity of reference (41) is the average velocity calculated based on its Figure 1b.



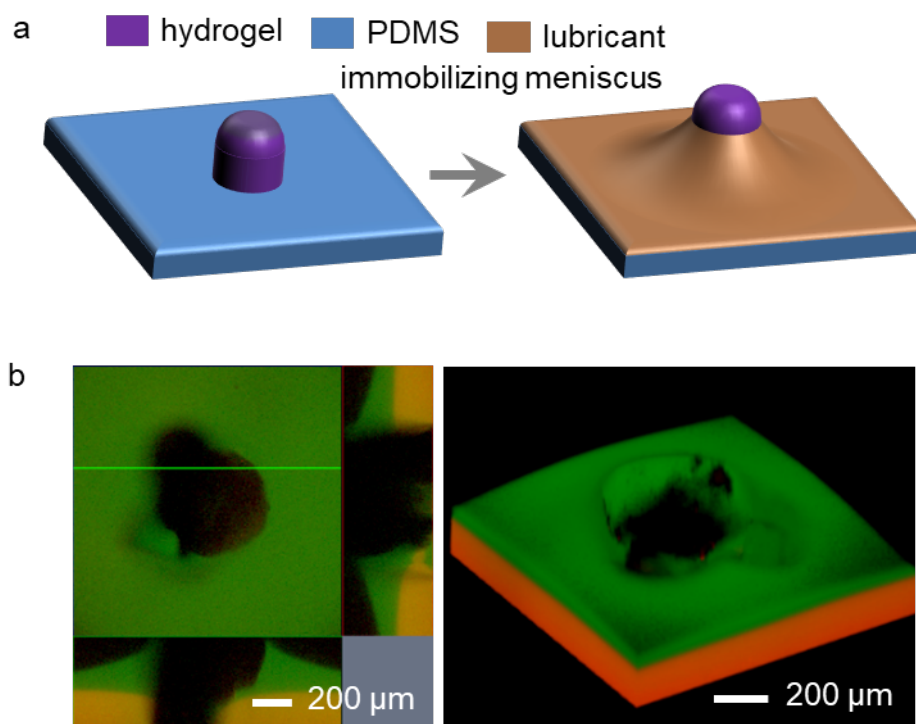


**Fig. S1 Immobilized lubricant meniscus is formed around the surface-piercing hydrogel dot.** (a) Scheme illustrating the formation of a lubricant meniscus around the hydrogel dot after adding lubricant to the patterned surface. (b) Confocal microscope images showing the formation of an oil meniscus around the hydrogel dot.

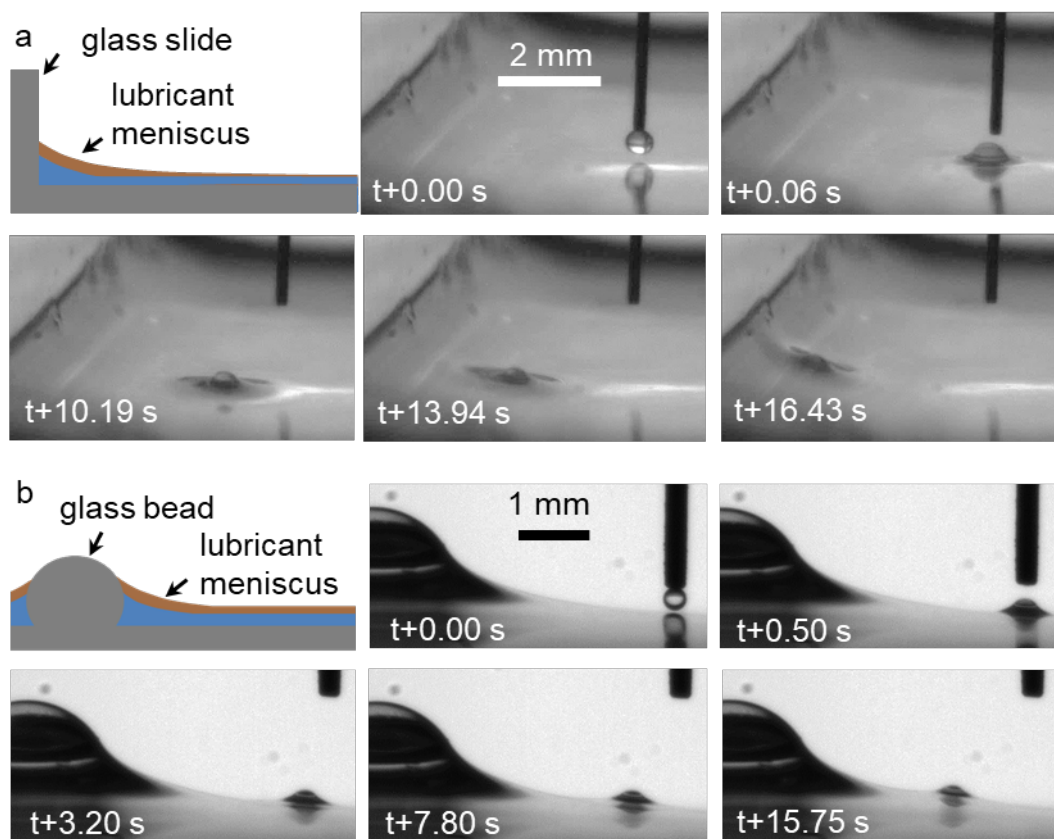


**Fig. S2 Driven of water microdroplets by lubricant menisci immobilized by a vertical glass slide (a) and a glass bead (b).** In both cases, the droplet could be driven by capillary pumping. The results indicate that the system is ubiquitous as long as a lubricant meniscus exists on the slippery surface.

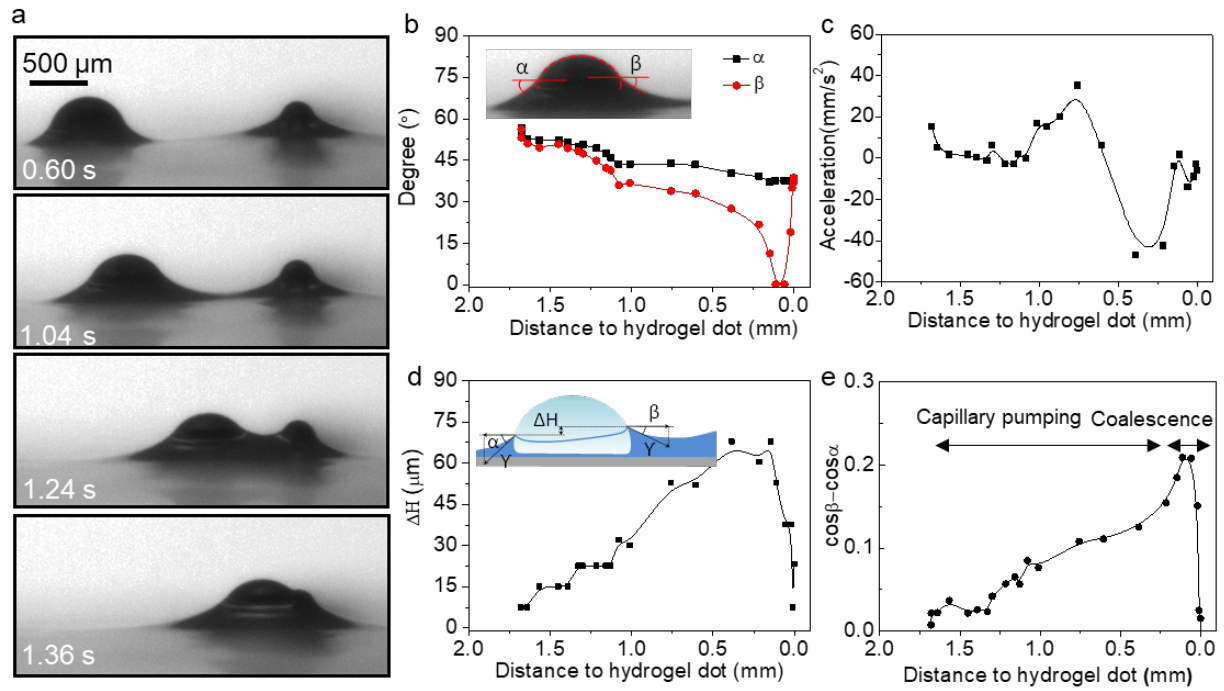


**Fig. S3 A typical droplet driving process.** (a) Time-lapsed microscope images showing a typical process to transport a microdroplet. The imbalance of lubricant wetting ridges increased as the droplet approaching the hydrogel dot. (b) The value of  $\alpha$  and  $\beta$  of the microdroplet in the driving process in (a). (c) The calculated acceleration of the microdroplet in (a). (d) The height difference of the oil layer at the two opposite edges of the microdroplet in (a). (e) The value of  $\cos\beta - \cos\alpha$  of the microdroplet as it was driven to the hydrogel dot in (a).  $\cos\beta - \cos\alpha$  represents the capillary force, which increases with the decreasing of distance, qualitatively in agreement with the prediction that  $F_c \propto \lambda/L$ . Note that  $F_c$  is estimated to be in the order of  $10^{-6}$  N, corresponding to an acceleration in the order of  $\text{m/s}^2$ . This is dramatically larger than the values in (c), suggesting that the capillary force is indeed largely balanced by viscous drag force, as we discussed in the main text.

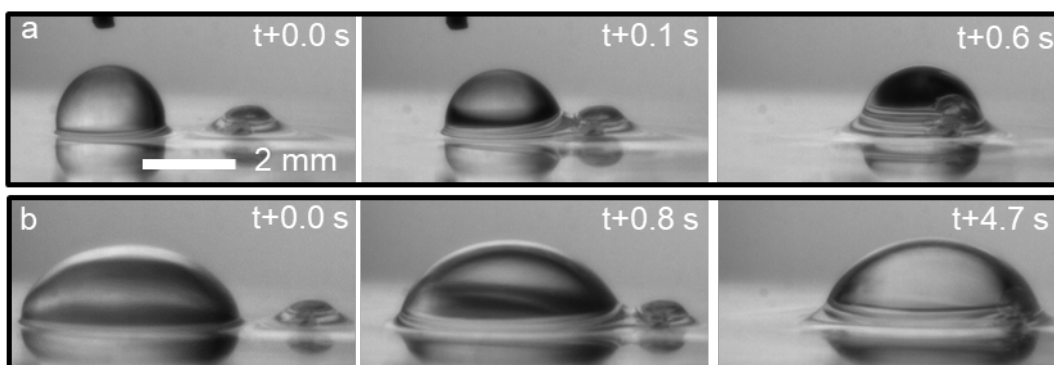


**Figure S4 Successful driven of relatively large droplet by the capillary pumping system.** Droplets with diameter of around 2 mm (a) and 5 mm (b) were driven to the hydrogel dot, respectively, demonstrates the driving system is also applicable for large droplets.

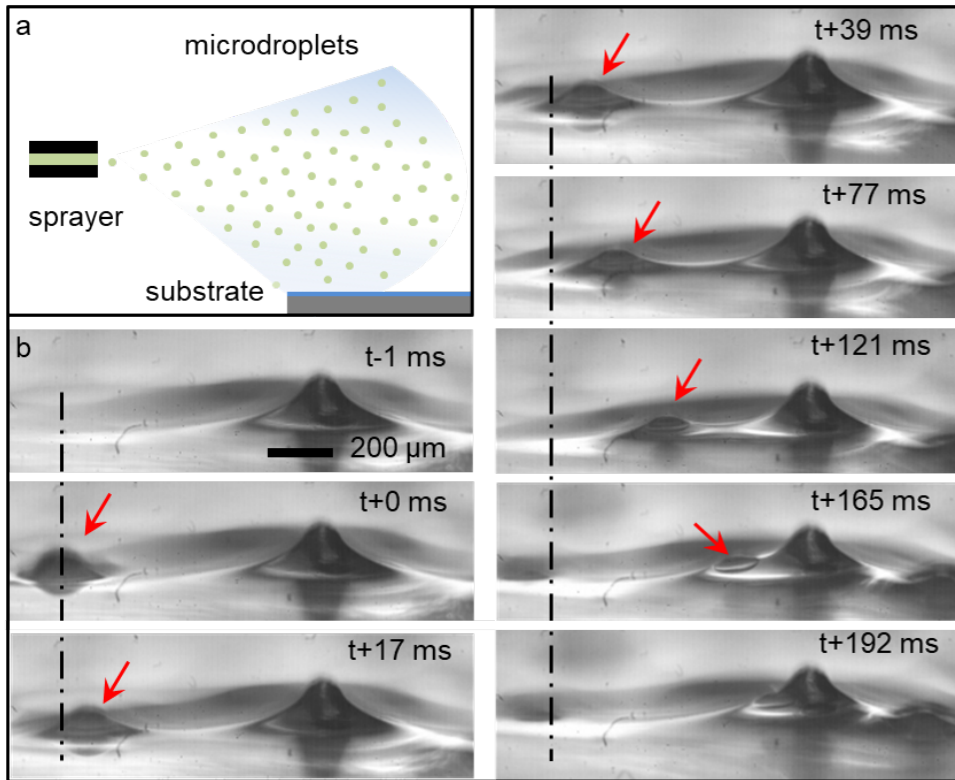


**Fig. S5 Driven of an aerosolized tiny droplet with a diameter of  $\sim 100 \mu\text{m}$ .** (a) Scheme showing the experimental setup. (b) Time-lapsed images captured by a high-speed camera showing a single aerosolized microdroplet with diameter of  $\sim 100 \mu\text{m}$  was driven to the hydrogel dot.

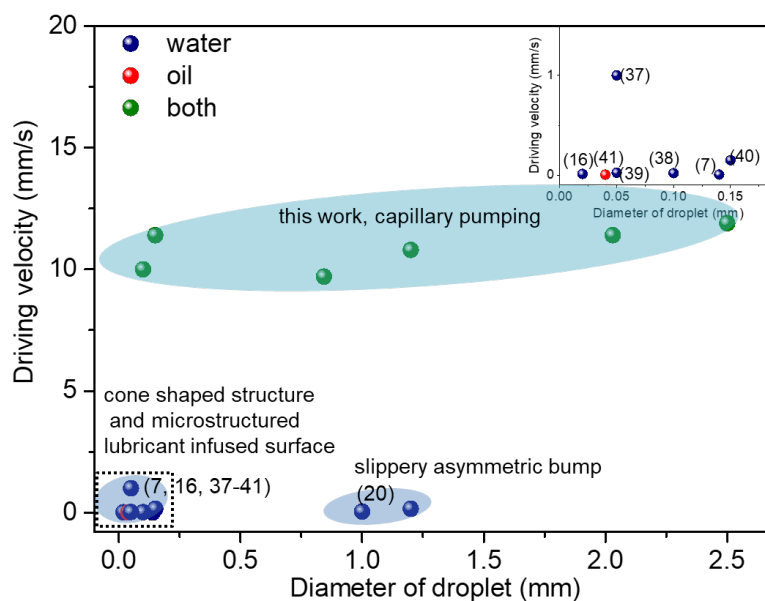


**Fig. S6** Comparison of the droplet diameter and highest driving velocity between our work and some other *bio-inspired droplet driven systems* that are capable to driven droplets with small sizes (7, 16, 20, 37-41). Our system is featured with driving of both water and oil microdroplets, driving droplets with a wide range of diameters, and driving droplet at a relatively high speed. The first driven system compared is the cone-shaped structure (including spider-silk-inspired fiber and cactus-spine-inspired needle) followed by two driven systems mainly inspired from pitch plant including nanostructured slippery surface and slippery asymmetric bump. Calculation of the highest velocity of previous systems and our system is shown in the Experiment Details of Supporting Information.

**Table S1** Comparison of the performance of this capillary pumping system with other droplet driving systems (4, 7, 9, 12, 16, 20, 37, 38, 40-48). Only our system is capable of driving both submillimeter-sized water and oil droplets.

	<b>Driving strategy or system</b>	<b>Water/oil</b>	<b>Minimum droplet diameter (mm)</b>	<b>Reference</b>
Plenary surface	Surface-energy- gradient surface	Water	1.50	(4)
		Water	2.30	(9)
		Water	1.50	(43)
		Water and oil	4.00	(44)
		Water	2.00	(45)
		Water	4.20	(46)
	Structure-gradient surface	Water and oil	2.20	(12)
		Water	1.90	(42)
Water		3.00	(47)	
Water		1.50	(48)	
Curvature surface	Cone-shaped fiber (coalescence is needed to drive droplet)	Water	0.14	(7)
		Water	0.02	(16)
		Water	0.05	(37)
		Water	0.15	(40)
		Water	0.10	(38)
		Oil	0.04	(41)
	Slippery asymmetric bump (coalescence is needed to drive droplet)	Water	1.20	(20)
	Microstructured lubricant-infused surface (coalescence is needed to drive the droplet)	Water	0.05	(39)
Capillary pumping on slippery surface	Water and oil	Minimum 0.15 mm tested. Essentially there should be no limit.	This work	

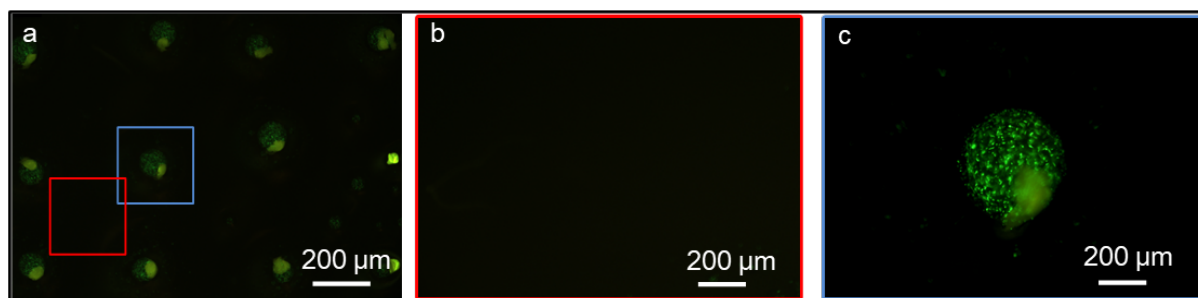


**Fig. S7 Collection of aerosolized GFP-tagged *E. coli* by a 3×4 hydrogel dot array for multi-site enrichment and analysis.** (a) Fluorescent microscope images showing the bacteria is successfully collected by the hydrogel dot array. Area outside the hydrogel dot keeps anti-fouling (b), while bacteria is collected to the hydrogel dot (c).

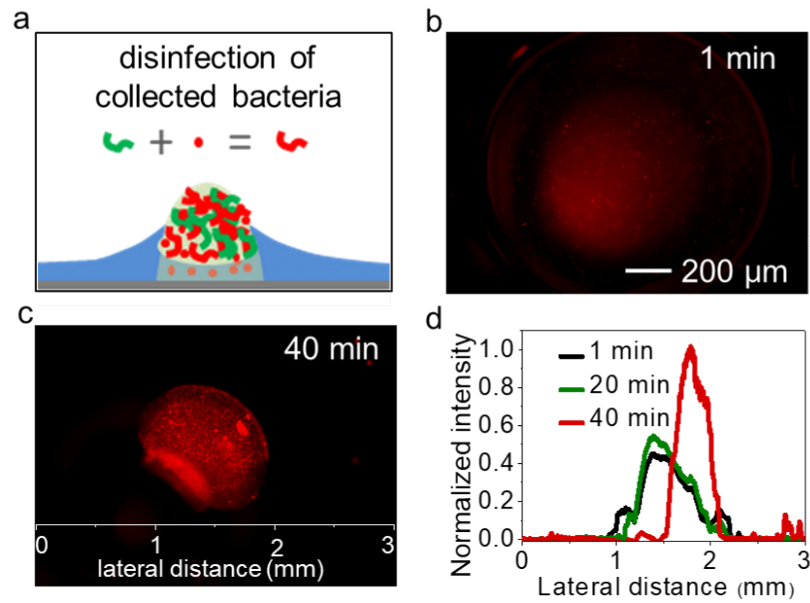


**Fig. S8 Killing enriched bacteria via pre-immobilization of a biocide of thyme essential oil on the hydrogel dot.** (a) A hydrogel dot loaded with thyme essential oil as biocide to disinfect collected bacteria. (b) and (c) Fluorescent microscope images showing the successful disinfection of collected bacteria. The red color indicates the dead bacteria stained with bacterial viability kit. (d) Measured fluorescent intensity at different time points of the disinfection process, suggesting the killing process.